# Sub-bandgap voltage electroluminescence and magneto-oscillations in a WSe2 light-emitting van der Waals heterostructure

## Citing this paper

## General rights

## Takedown policy

OPEN ACCESS

# Sub-bandgap voltage electroluminescence and magneto-oscillations in a WSe$_2$ light-emitting van der Waals heterostructure

Johannes Binder,[*,†,‡] Freddie Withers,[¶,§] Maciej R. Molas,[†] Clement Faugeras,[†] Karol Nogajewski,[†] Kenji Watanabe,[‖] Takashi Taniguchi,[‖] Aleksey Kozikov,[¶,§] Andre K. Geim,[§,⊥] Kostya S. Novoselov,[¶,§] and Marek Potemski[*,†]

†*Laboratoire National des Champs Magnetiques Intenses, CNRS-UGA-UPS-INSA-EMFL, 25 Rue des Martyrs, 38042 Grenoble, France*

‡*Faculty of Physics, University of Warsaw, Pasteura 5, 02-093 Warsaw, Poland*

¶*School of Physics and Astronomy, University of Manchester, Oxford Road, Manchester M13 9PL, UK*

§*National Graphene Institute, University of Manchester, Oxford Road, Manchester, M13 9PL, UK*

‖*National Institute for Materials Science, 1-1 Namiki, Tsukuba 305-0044, Japan*

⊥*Manchester Centre for Mesoscience and Nanotechnology, University of Manchester, Oxford Road, Manchester, M13 9PL, UK*

E-mail: johannes.binder@fuw.edu.pl; marek.potemski@lncmi.cnrs.fr

Phone: +48 22 55 32 792; +33 476 88 78 76

## Abstract

We report on experimental investigations of an electrically driven WSe$_2$ based light-emitting van der Waals heterostructure. We observe a threshold voltage for electrolu-

1

minescence significantly lower than the corresponding single particle band gap of mono-layer $WSe_2$. This observation can be interpreted by considering the Coulomb interaction and a tunneling process involving excitons, well beyond the picture of independent charge carriers. An applied magnetic field reveals pronounced magneto-oscillations in the electroluminescence of the free exciton emission intensity with a 1/B-periodicity. This effect is ascribed to a modulation of the tunneling probability resulting from the Landau quantization in the graphene electrodes. A sharp feature in the differential conductance indicates that the Fermi level is pinned and allows for an estimation of the acceptor binding energy.

# Keywords

electroluminescence, magneto-oscillations, van der Waals heterostructures, tungsten dise-lenide, hexagonal boron nitride, acceptor

A new step of complexity has recently been undertaken in the field of two-dimensional crystals, by deterministically placing atomically thin layers of different materials on top of each other. The resulting stacks are referred to as van der Waals (vdW) heterostructures.[1,2] Based on this idea, a few prototype devices, such as tunneling transistors[3–11] and/or light-emitting tunneling diodes,[12–16] have been fabricated and successfully tested. However, further work is necessary in order to better characterize such structures, to learn more about their electronic and optical properties, with the aim to properly design device operation.

Here, we unveil new facets of light emitting vdW heterostructures, with reference to the issue of the alignment of electronic bands, effects of Coulomb interaction and a subtle but still active role of the graphene electrodes in these devices. We report on optoelectronic measurements performed on a $WSe_2$-based tunneling light-emitting diode. The differential tunneling conductance of our structure shows a large zero bias anomaly (peak), which we ascribe to pinning of the Fermi energy at the $WSe_2$ impurity/acceptor level. A conceivable scenario for the evolution of the band alignment as a function of the bias voltage is proposed.

Strikingly, the bias-potential onset for the electroluminescence is found to coincide with the energy of the free exciton of the WSe$_2$ monolayer (and not with the energy of a single-particle bandgap). This fact points out the relevant role of Coulomb interactions between electrically injected carriers on the tunneling processes in our device. Furthermore, pronounced magneto-oscillations are observed in the electroluminescence emission intensity measured as a function of magnetic field applied perpendicularly to the layer planes. These oscillations, periodic with the inverse of the magnetic field, reflect the modulation of the efficiency of carrier tunneling and are caused by the Landau quantization of the two-dimensional graphene electrodes.

We studied a light-emitting diode structure[12,13] that is based on a WSe$_2$ monolayer as the active part. The layer sequence for this device was Si / SiO$_2$ / hBN / graphene / hBN / WSe$_2$ / hBN / graphene. The emission area of the structure is presented on the microscope image in Figure 1 (a). Figure 1 (b) depicts a schematic drawing of the layered structure. The two hBN spacers that separate the WSe$_2$ monolayer from the graphene electrodes are two layers thick. A detailed description of the fabrication process can be found in Ref. [12].

The optoelectronic characteristics of the sample were studied by recording the electro-luminescence (EL) signal as a function of bias voltage and in magnetic fields up to 14 T. Current-voltage curves were measured to study the tunneling processes and photolumines-cence (PL) mapping of the sample was performed to additionally characterize the structure. All measurements were performed with an optical-fiber-based insert placed in a supercon-ducting coil. The investigated sample was located on top of an x-y-z piezo-stage kept in helium gas at $T = 4.2$ K. The laser light from a continuous wave Ar+ laser ($\lambda = 514.5$ nm) was coupled to an excitation fiber of 5 $\mu$m diameter, focused on the sample by an aspheric lens. The signal was detected with a 50 $\mu$m core fiber (collection spot diameter of $\sim 10$ $\mu$m) by a 0.5 m long monochromator equipped with a charge-couple-device (CCD) camera. Elec-trical measurements were performed using a Keithley 2400 source-measure unit.

A vertical current was observed upon the application of a bias voltage (V$_b$) between the two graphene electrodes. Such a charge transfer from one graphene layer to the other can
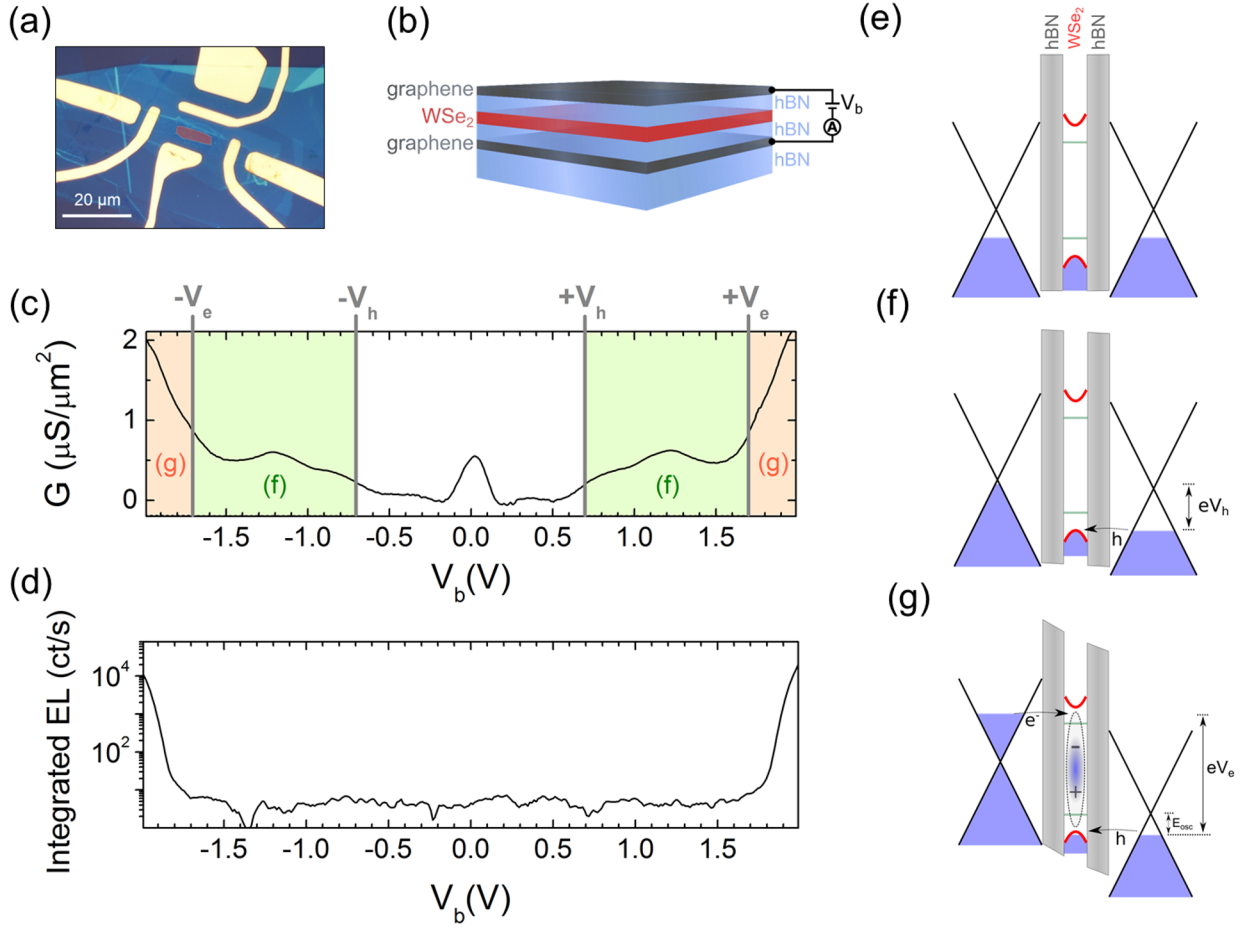
Figure 1: Device structure and transport characteristics. (a) Microscope image of the active part of the sample. The brown area indicates the position of the WSe$_2$ flake. (b) Schematic illustration of the heterostructure shown in (a). The layer sequence from bottom to top is hBN/graphene/hBN/WSe$_2$/hBN/graphene. (c) Differential conductance $G = dI/dV_b$. The colored regions correspond to the situation shown in (f) and (g). (d) Integrated EL signal in a spectral range from 1.48 eV to 1.85 eV as a function of the bias voltage. (e) Schematic band diagram for zero bias. The red parabolic bands correspond to the K-point of the Brillouin zone in WSe$_2$. The horizontal green lines depict donor/acceptor-like bands. (f) Schematic band diagram for the case of intermediate bias. Here holes can tunnel through the hBN barrier into WSe$_2$, but electrons can not. $V_h$ corresponds to the voltage required to inject holes. (g) Band diagram for large bias. In this case, both holes and electrons can tunnel. $V_e$ stands for the voltage threshold for the tunneling of electrons into excitonic states of WSe$_2$. The exciton is depicted schematically. In this regime light emission is observed due to exciton recombination in the WSe$_2$ monolayer. $E_{osc}$ indicates the offset extracted from Eqn. 2.

4

only be achieved via tunneling. To describe the electronic transport perpendicular to the structure, we present in Figure 1 (c) the variations of the differential conductance $G=dI/dV_b$ as a function of the bias applied between the two graphene electrodes. The optical emission was monitored at the same time. The corresponding integrated EL intensity is presented in Figure 1 (d).

To interpret the optoelectronic behavior of this device, it is crucial to know the band alignment of the heterostructure. To this end one has to rely both on the theoretical esti-mations[17,18] and on the spectroscopic experimental works targeting these band offsets.[3,5,19] A schematic illustration of the bands is shown in Figure 1 (e). The drawing depicts the two graphene electrodes, represented by Dirac cones, which are separated from the WSe$_2$ monolayer by the hBN barriers. The WSe$_2$ layer is schematically illustrated by the parabolic bands around the K-point of the Brillouin zone. In addition donor/acceptor-like bands are depicted by horizontal green lines in WSe$_2$. Transport measurements of the tunneling cur-rent in hBN/graphene/hBN structures found the valence band of hBN to be offset by about $1.4 - 1.5$ eV[3,5] from the graphene Dirac point. The band alignment of monolayer WSe$_2$ and graphene has been recently studied using $\mu$-ARPES and an offset of 0.70 eV between the Dirac point and the WSe$_2$ valence band edge has been reported.[19] Assuming a direct band gap for monolayer WSe$_2$ of about $2 - 2.2$ eV[20,21] one can conclude that the energy separation between the Dirac point of graphene and the valence band edge of WSe$_2$ should be significantly lower as compared to the conduction band. This finding is also in agreement with theoretical estimations.[17,18] The results are summarized qualitatively in the sketch in Figure 1 (e).

By using the proposed band alignment scenario, we can divide the differential conduc-tance (Figure 1 (c)) in three distinct tunneling regimes. The first one occurs at around zero bias, where a pronounced peak is observed. We ascribe this feature to be caused by the tun-neling through impurity donor/acceptor bands in WSe$_2$, that pin the Fermi level (Figure 1 (e)). With an increase in bias voltage the tunneling through the impurity band ceases to be

resonant and a decrease in differential conductance is observed, giving rise to a symmetric peak-like shape. Our measurements cannot directly infer whether these impurities are of donor or acceptor type. However, within the expected band alignment, the Dirac point of graphene is much closer in energy to the valence band edge of $WSe_2$, a material which shows preferably p-type conductivity.[22-26] Hence, we assume that the dominant impurities in the investigated $WSe_2$ monolayer are of acceptor type, and that the Fermi level is pinned to this impurity band at zero applied bias. A small applied bias is then sufficient to move the Fermi levels of the graphene electrodes out of resonance with this band, producing a symmetric differential conductance feature centered at zero applied bias. The peak at zero bias was also observed for other similar $WSe_2$ devices, however it was found that its magnitude can strongly vary from device to device (see supporting information) and it can also be absent. This variation can be understood in terms of different unintentional initial doping of $WSe_2$, which might vary from flake to flake.

The second regime, indicated by the green color in Figure 1 (c), shows an overall increase of conductance with two peak-like features. The first feature, around $V_h \sim \pm 0.7$ V, originates from the onset of hole tunneling into the valence band of $WSe_2$. This process becomes efficient when the Fermi level of one graphene layer is moved by the amount of the acceptor binding energy, to coincide with the valence band edge of $WSe_2$. The situation is schematically depicted in Figure 1 (f). At this point one should mention that another possible reason for the above mentioned peak at zero bias could be resonant effects due to the direct graphene-graphene tunneling.[27] However, the graphene electrodes were not intentionally aligned, making the appearance of resonant effects very improbable. Another argument against this alternative scenario is that with a Femi level close to the Dirac point, one would roughly need to apply a voltage corresponding to twice the valence band offset to enable hole tunneling, which does not fit the observation of $V_h \sim \pm 0.7$ V. The second feature in this regime is the peak at larger bias voltage ($V_d \sim \pm 1.2$ V). The origin of this peak is still unclear, and a possible explanation could be tunneling involving mid-gap impurity states in

WSe$_2$.

The above discussion yields three conditions: an onset voltage for hole tunneling of $V_h \sim \pm 0.7$ V, a valence band offset for monolayer WSe$_2$ of E$_{VB} \sim 0.7$ eV, and a Fermi level that is pinned at zero applied bias to the acceptor level. These conditions together with simple considerations regarding the band structure and the electric field in the sample allows us to estimate an acceptor binding energy of $E_{acc} \sim 250$ meV (see supporting information).

At larger bias (third regime) the increase in voltage will mostly drop across the graphene / hBN junction that does not permit tunneling into the WSe$_2$ layer. In order to observe EL, both electrons and holes must be present in the WSe$_2$ layer. This condition is satisfied in the voltage region around $V_e \sim \pm 1.7$ V above which EL is observed. The voltage dependence of the spectrally integrated EL signal, shown in Figure 1 (d), displays a steep onset of emission in that bias range. We can therefore ascribe the strong increase in conductance to the tunneling of electrons into the WSe$_2$ monolayer (compare Figure 1 (g)). Additional data for a similar device showing the same behavior is presented in the supporting information. Strikingly, the onset for EL of $V_e \sim \pm 1.7$ V is significantly smaller as compared to the direct band gap of a WSe$_2$ monolayer which is of about $2 - 2.2$ eV.[20,21] Because the base temperature of our experiment $T = 4.2$ K implies a thermal energy below 400 $\mu$eV and given the relative alignment of the graphene electronic bands with respect to those of hBN, the large difference can hardly be explained in terms of thermal activation of carriers or a lowering of the effective hBN barrier caused be the electric field. However, the EL onset at about $V_e \sim \pm 1.7$ V corresponds well with the emitted free exciton energy of $\sim 1.72$ eV. Based on our experiments, the most probable scenario involves tunneling[28] directly into the excitonic states of the WSe$_2$ monolayer. Because the tunneling of holes starts at bias voltages close to $V_h \sim \pm 0.7$ V, a population of holes is already present in the valence band when electrons start to tunnel, directly forming excitons. Such processes were indeed observed for resonant electron tunneling into p-doped GaAs quantum wells (QWs).[29] In the case of WSe$_2$ monolayer, the exciton binding energies are large ($\sim 0.4$ eV[20]) as compared to excitons

in GaAs QW systems, which gives rise to the observed large differences. Moreover, it was shown that excitons can persist in such materials up to large carrier concentrations,[30] with an estimation of several $10^{13}$ cm$^{-2}$ required for the quenching of the excitonic resonances.[31]

Figure 2 (a) shows representative PL and EL spectra. The highest energy band ($E \sim$ 1.72 eV) labelled X$^0$ can be attributed to the neutral, free A exciton resonance. As observed in EL, the X$^0$ feature has a full width at half maximum (FWHM) close to 20 meV, hence 3 to 4 times bigger than in PL (red dashed line in Fig. 2 (a)). The large FWHM originates from inhomogeneous broadening, which is more apparent in EL than PL since in the case of the former the signal is collected from the entire flake. At lower energies, a complex broad band is observed, typical for monolayer WSe$_2$ samples and which has been attributed to charged and localized (bound) excitons.[13,32–34] This large broad band indicates the presence of a significant amount of impurities in the case of our device. The presence of defects as evidenced by the optical measurements fits into the scenario of a pinned Fermi level for this device. A magnetic field was applied perpendicular to the surface of the structure in order to study its impact on the EL signal. First, a strong magneto-resistance develops in the structure and significantly shifts the threshold bias for EL emission to larger voltages with increasing applied magnetic field. We ascribe this additional resistance to be caused by the in-plane magneto-resistance of the graphene contacts, which serve as conductors between the metal contacts and the active area.[9] This effect hinders measurements with constant applied voltage. To compensate for the additional voltage drop a constant current was kept for the magnetic field sweeps, which yielded stable EL measurement conditions.

Figure 2 (b) shows a three-dimensional false color plot of the raw EL signal as a function of magnetic field. We observed a very intense modulation of the X$^0$ line with an intensity and a shape that varies as a function of the magnetic field. This modulation of the exciton emission is not a simple on-off effect, but due to the large width of the X$^0$ feature in EL, an energy-dependent modulation of the X$^0$ emission can be observed. In order to establish the origin of the modulations, a cut at a constant energy of the X$^0$-feature plotted as $1/B$
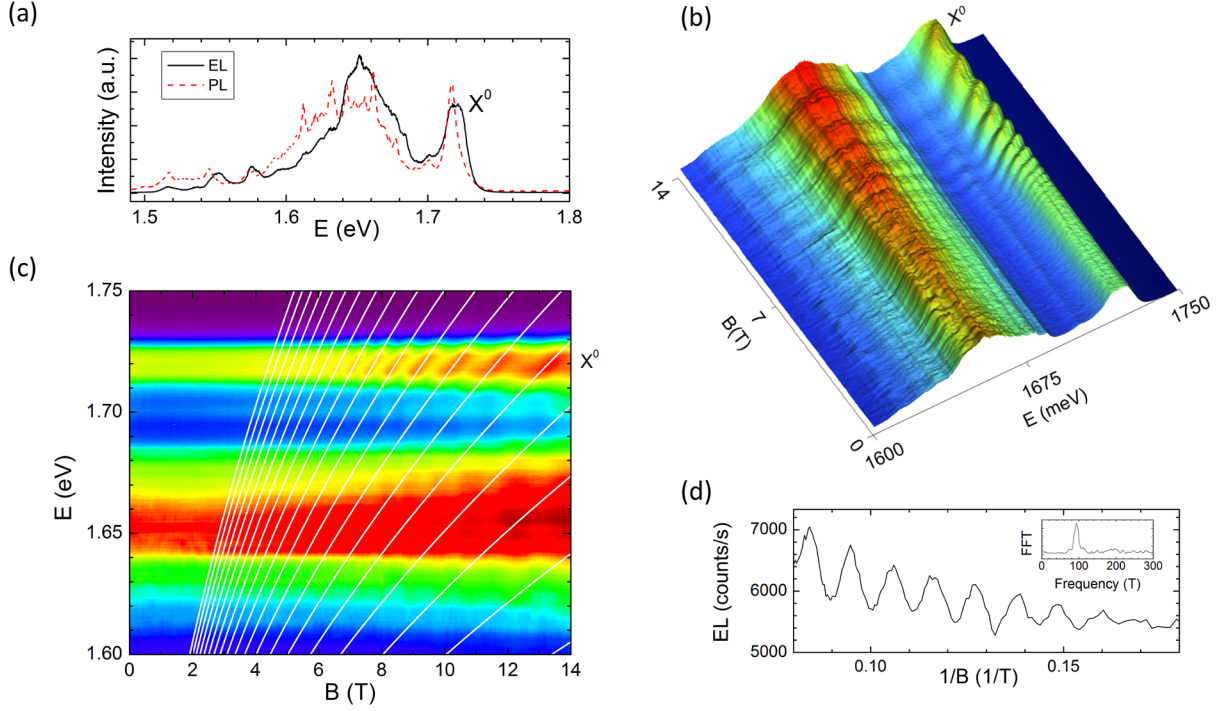
8

Figure 2: Optical characteristics in magnetic field. (a) Representative EL - (black line) and PL - (red dashed line) spectra for $B = 0$. (b) Three dimensional false color plot of the raw EL signal as a function of the magnetic field for a constant current of I=36 $\mu A$. (c) Overlay of the two-dimensional EL false color map with the graphene Landau level spectrum (white lines). The graphene LL spectrum was calculated using $v_f = 1 \cdot 10^6 \frac{m}{s}$ and an energy offset for the Dirac point of $E_d = 350$ meV as deduced from the observed periodicity of 93 T. (d) Horizontal cut to (c) at $E = 1.72$ eV (neutral exciton) as a function of $1/B$. Inset: result of the Fourier analysis that shows a sharp peak at 93 T.

is presented in Figure 2 (d). A $1/B$-periodicity is apparent, which is further supported by the results of a Fourier analysis for this graph giving a well defined peak for a period $\Delta(1/B) = 93$ T (see inset). Assuming Landau quantization in the graphene electrodes to be responsible for the observed behavior, one obtains the following Landau level (LL) spectrum[35,36]

$$E_n = sign(n)v_f\sqrt{2e\hbar B|n|} \tag{1}$$

where $v_f = 1 \cdot 10^6 \frac{m}{s}$ is the Fermi velocity and $n$ the Landau level index. For a constant energy cut across the LL-spectrum of graphene, one obtains oscillations with a $1/B$ periodicity. Hence, by using the extracted periodicity one can determine the energy above the Dirac point by calculating

$$E_{osc} = v_f\sqrt{\frac{2e\hbar}{\Delta(\frac{1}{B})}} \tag{2}$$

This consideration yields an energy separation of about $E_{osc} = 350$ meV. In Figure 2 (c) we present an overlay of the graphene Landau levels with the Dirac point located 350 meV below the energy of the $X^0$ line and the measured EL-spectra. We find an excellent agreement, since the spacing as well as the energy dependence of the modulations are fully described. Consequently, we conclude that the oscillations are related to the quantized density of states (DOS) of the graphene electrodes. This quantization leads to oscillations in the population of holes in the $WSe_2$ valence band, since the injection process via tunneling from graphene is modulated by the LL spectrum. At lower energies, no signatures of an energy-dependent modulation could be observed for the broad localized (bound) exciton emission band. However, an attenuation of the broad band that oscillates with the magnetic field but not with the energy is apparent when the exciton is affected by the above discussed tunneling process. Such a behavior can be observed in Figure 2 (b) and (c) in the form of lines on top of the broad emission band. This effect is more markedly shown in Figure 3,

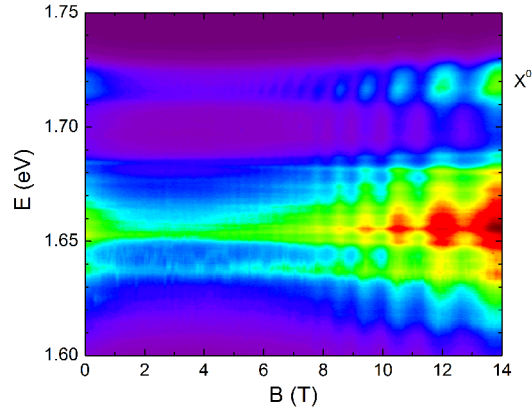which presents an EL false color map at lower injection current.



Figure 3: Oscillations of the localized excitonic bands. Two-dimensional false color map of the magnetic field dependence of the EL signal for a constant current of $I = 30 \mu A$. The vertical streaks indicate the transfer of periodicity from the free exciton line $X^0$ to the localized excitonic bands.

This effect confirms that the population of these localized states is fed by the population of free excitons: electrons are injected into the $WSe_2$ layer via tunneling and directly bound to holes to first form excitons which can scatter to the localized excitonic bands, at lower energy.[37] As a consequence, instead of an energy-dependent modulation, as it was observed for the broadened $X^0$ line, one would expect the oscillation frequency to be transferred from the free exciton to the localized bands.

Another characteristic observation is the appearance of a single frequency although there are two tunneling processes (holes and electrons) with different tunneling barriers. Eqn. 1 describes a Landau level fan chart with an energy spacing between consecutive LLs that decreases with increasing LL-index n. This implies that for a high Fermi energy, the LL spectrum can be significantly smeared out, thus no clear oscillatory behavior can be expected concerning the electron tunneling. This observation of a single frequency modulating the exciton emission intensity, can therefore be seen as an additional evidence that the graphene electrodes are responsible for the oscillations. The modulation in tunneling that was registered optically should in principle also be present in the electrical characteristics. Instead, the experiment shows no clear modulation in the measured voltage as a function

of magnetic field. This discrepancy can be understood when taking into account the actual processes that influence the two measurement techniques. The EL signal is only sensitive to the excitonic population, which is a result of the injection of electrons and holes via tunneling. The electrical measurement, however, is a sum of all possible tunneling pathways and does also include leakage and parasitic components, which can mask the effect. With the magneto-EL measurement we therefore gained information difficult to access with standard magneto-transport tunneling experiments.

In summary, we report on optoelectronic properties of a $WSe_2$ based tunneling light-emitting vdW heterostructure in magnetic fields. We propose a conceivable scenario for the band alignment in the structure, which allows us to estimate an acceptor binding energy. The Landau quantization in the graphene electrodes is shown to strongly modulate the injection of holes into the valence band of the active $WSe_2$ monolayer, which in turn modulates the EL signal. The observed oscillations of the neutral exciton intensity as a function of the magnetic field show a pronounced $1/B$ periodicity which was used to deduce an effective band offset between graphene's Dirac point and the valence band edge of the $WSe_2$ monolayer. Our results hence show that the role of graphene electrodes in vdW heterostructures goes far beyond being a semitransparent electrode with a low density of states.

In addition, we observed EL emission for applied voltages well below the corresponding band gap of monolayer $WSe_2$, which was explained in terms of direct tunneling of carriers into excitonic states in $WSe_2$. We found the EL signal to be more sensitive to the quantized hole injection as compared to magneto-transport, which illustrates the advantage of optoelectronic tunneling measurements. Our findings highlight the importance of excitonic states for the tunneling processes in vdW heterostructures, giving rise to sub-bandgap EL, which could be a key aspect for future optoelectronic device engineering.

# Acknowledgement

# Supporting Information

Band structure and electric field considerations, additional data on the zero bias anomaly on other samples, evolution of the electroluminescence as a function of bias voltage for a different sample.

# References

(1) Geim, A.; Grigorieva, I. *Nature* **2013**, *499*, 419–425.

(2) Novoselov, K. S.; Mishchenko, A.; Carvalho, A.; Castro Neto, A. H. *Science* **2016**, *353*.

(3) Britnell, L.; Gorbachev, R. V.; Jalil, R.; Belle, B. D.; Schedin, F.; Mishchenko, A.; Georgiou, T.; Katsnelson, M. I.; Eaves, L.; Morozov, S. V.; Peres, N. M. R.; Leist, J.; Geim, A. K.; Novoselov, K. S.; Ponomarenko, L. A. *Science* **2012**, *335*, 947.

(4) Georgiou, T.; Jalil, R.; Belle, B. D.; Britnell, L.; Gorbachev, R. V.; Morozov, S. V.; Kim, Y.-J.; Gholinia, A.; Haigh, S. J.; Makarovsky, O.; Eaves, L.; Ponomarenko, L. A.; Geim, A. K.; Novoselov, K. S.; Mishchenko, A. *Nat. Nanotechnol.* **2013**, *8*, 100–103.

(5) Zhao, Y.; Wan, Z.; Xu, X.; Patil, S.; Hetmaniuk, U.; Anantram, M. *Sci. Rep.* **2015**, *5*, 10712.

(6) Mishchenko, A. et al. *Nat. Nanotechnol.* **2014**, *9*, 808–813.

(7) Lin, Y.-C.; Ghosh, R. K.; Addou, R.; Lu, N.; Eichfeld, S. M.; Zhu, H.; Li, M.-Y.; Peng, X.; Kim, M. J.; Li, L.-J.; Wallace, R. M.; Datta, S.; Robinson, J. A. *Nat. Commun.* **2015**, *6*, 7311.

(8) Roy, T.; Liu, L.; de la Barrera, S.; Chakrabarti, B.; Hesabi, Z.; Joiner, C.; Feenstra, R.; Gu, G.; Vogel, E. *Appl. Phys. Lett.* **2014**, *104*, 123506.

(9) Greenaway, M. T.; Vdovin, E. E.; Mishchenko, A.; Makarovsky, O.; Patane, A.; Wallbank, J. R.; Cao, Y.; Kretinin, A. V.; Zhu, M. J.; Morozov, S. V.; Falko, V. I.; Novoselov, K. S.; Geim, A. K.; Fromhold, T. M.; Eaves, L. *Nat. Phys.* **2015**, *11*, 1057–1062.

(10) Gaskell, J.; Eaves, L.; Novoselov, K.; Mishchenko, A.; Geim, A.; Fromhold, T.; Greenaway, M. *Appl. Phys. Lett.* **2015**, *107*, 103105.

(11) Wallbank, J. R. et al. *Science* **2016**, *353*, 575.

(12) Withers, F.; Del Pozo-Zamudio, O.; Mishchenko, A.; Rooney, A. P.; Gholinia, A.; Watanabe, K.; Taniguchi, T.; Haigh, S. J.; Geim, A. K.; Tartakovskii, A. I.; Novoselov, K. S. *Nat. Mater.* **2015**, *14*, 301–306.

(13) Withers, F. et al. *Nano Lett.* **2015**, *15*, 8223–8228.

(14) Clark, G.; Schaibley, J. R.; Ross, J.; Taniguchi, T.; Watanabe, K.; Hendrickson, J. R.; Mou, S.; Yao, W.; Xu, X. *Nano Lett.* **2016**, *16*, 3944–3948.

(15) Palacios-Berraquero, C.; Barbone, M.; Kara, D. M.; Chen, X.; Goykhman, I.; Yoon, D.; Ott, A. K.; Beitner, J.; Watanabe, K.; Taniguchi, T.; Ferrari, A. C.; Atature, M. *Nat. Commun.* **2016**, *7*, 12978.

(16) Schwarz, S.; Kozikov, A.; Withers, F.; Maguire, J. K.; Foster, A. P.; Dufferwiel, S.; Hague, L.; Makhonin, M. N.; Wilson, L. R.; Geim, A. K.; Novoselov, K. S.; Tartakovskii, A. I. *2D Mater.* **2016**, *3*, 025038.

(17) Gong, C.; Zhang, H.; Wang, W.; Colombo, L.; Wallace, R. M.; Cho, K. *Appl. Phys. Lett.* **2013**, *103*, 053513.

(18) Kang, J.; Tongay, S.; Zhou, J.; Li, J.; Wu, J. *Appl. Phys. Lett.* **2013**, *102*, 012111.

(19) Wilson, N. R.; Nguyen, P. V.; Seyler, K. L.; Rivera, P.; Marsden, Z. P. L., A. J.and Laker; Constantinescu, V., G. C.and Kandyba; Barinov, A.; Hine, N. D. M.; Xu, X.; H. Cobden, D. H. *http://arxiv.org/abs/1601.05865* **2016**,

(20) He, K.; Kumar, N.; Zhao, L.; Wang, Z.; Mak, K. F.; Zhao, H.; Shan, J. *Phys. Rev. Lett.* **2014**, *113*, 026803.

(21) Zhang, C.; Chen, Y.; Johnson, A.; Li, M.-Y.; Li, L.-J.; Mende, P. C.; Feenstra, R. M.; Shih, C.-K. *Nano Lett.* **2015**, *15*, 6494–6500.

(22) Fang, H.; Chuang, S.; Chang, T. C.; Takei, K.; Takahashi, T.; Javey, A. *Nano Lett.* **2012**, *12*, 3788–3792.

(23) Pradhan, N. R.; Rhodes, D.; Memaran, S.; Poumirol, J. M.; Smirnov, D.; Talapatra, S.; Feng, S.; Perea-Lopez, N.; Elias, A. L.; Terrones, M.; Ajayan, P. M.; Balicas, L. *Sci. Rep.* **2015**, *5*, 8979.

(24) Movva, H. C.; Rai, A.; Kang, S.; Kim, K.; Fallahazad, B.; Taniguchi, T.; Watanabe, K.; Tutuc, E.; Banerjee, S. K. *ACS nano* **2015**, *9*, 10402–10410.

(25) Fallahazad, B.; Movva, H. C. P.; Kim, K.; Larentis, S.; Taniguchi, T.; Watanabe, K.; Banerjee, S. K.; Tutuc, E. *Phys. Rev. Lett.* **2016**, *116*, 086601.

(26) Campbell, P. M.; Tarasov, A.; Joiner, C. A.; Tsai, M.-Y.; Pavlidis, G.; Graham, S.; Ready, W. J.; Vogel, E. M. *Nanoscale* **2016**, *8*, 2268–2276.

(27) Britnell, L.; Gorbachev, R.; Geim, A.; Ponomarenko, L.; Mishchenko, A.; Greenaway, M.; Fromhold, T.; Novoselov, K.; Eaves, L. *Nat. Commun.* **2013**, *4*, 1794.

(28) Geim, A. K.; Main, P. C.; La Scala, N.; Eaves, L.; Foster, T. J.; Beton, P. H.; Sakai, J. W.; Sheard, F. W.; Henini, M.; Hill, G.; Pate, M. A. *Phys. Rev. Lett.* **1994**, *72*, 2061.

(29) Cao, H.; Klimovitch, G.; Björk, G.; Yamamoto, Y. *Phys. Rev. Lett.* **1995**, *75*, 1146.

(30) Scharf, B.; Wang, Z.; Tuan, D. V.; Shana, J.; Mak, K. F.; Zutic, I.; Dery, H. *http://arxiv.org/abs/1606.07101* **2016**,

(31) Chernikov, A.; van der Zande, A. M.; Hill, H. M.; Rigosi, A. F.; Velauthapillai, A.; Hone, J.; Heinz, T. F. *Phys. Rev. Lett.* **2015**, *115*, 126802.

(32) Jones, A. M.; Yu, H.; Ghimire, N. J.; Wu, S.; Aivazian, G.; Ross, J. S.; Zhao, B.; Yan, J.; Mandrus, D. G.; Xiao, D.; Yao, W.; Xu, X. *Nat. Nanotechnol.* **2013**, *8*, 634–638.

(33) Arora, A.; Koperski, M.; Nogajewski, K.; Marcus, J.; Faugeras, C.; Potemski, M. *Nanoscale* **2015**, *7*, 10421–10429.

(34) Koperski, M.; Nogajewski, K.; Arora, A.; Cherkez, V.; Mallet, P.; Veuillen, J.-Y.; Marcus, J.; Kossacki, P.; Potemski, M. *Nat. Nanotechnol.* **2015**, *10*.

(35) Faugeras, C.; Amado, M.; Kossacki, P.; Orlita, M.; Kühne, M.; Nicolet, A.; Latyshev, Y. I.; Potemski, M. *Phys. Rev. Lett.* **2011**, *107*, 036807.

(36) Faugeras, C.; Binder, J.; Nicolet, A.; Leszczynski, P.; Kossacki, P.; Wysmolek, A.; Orlita, M.; Potemski, M. *EPL* **2014**, *108*, 27011.

(37) Wang, G.; Bouet, L.; Lagarde, D.; Vidal, M.; Balocchi, A.; Amand, T.; Marie, X.; Urbaszek, B. *Phys. Rev. B* **2014**, *90*, 075413.